Journal of Materials Science and Chemical Engineering, 2017, 5, 46-66
http://www.scirp.org/journal/msce
ISSN Online: 2327-6053
ISSN Print: 2327-6045

Synthesis and Characterization of Free and Copper (II) Complex of N,N′-*Bis*(Salicylidene)Ethylenediamine for Application in Dye Sensitized Solar Cells

William Ghann[1], Hany Sobhi[2*], Hyeonggon Kang[1], Tulio Chavez-Gil[3], Fred Nesbitt[3], Jamal Uddin[1*]

[1]Center for Nanotechnology, Department of Natural Sciences, Coppin State University, Baltimore, MD, USA
[2]Coppin Center for Organic Synthesis, Department of Natural Sciences, Coppin State University, Baltimore, MD, USA
[3]Inorganic and Physical Chemistry Lab, Department of Natural Sciences, Coppin State University, Baltimore, MD, USA
Email: *juddin@coppin.edu, *hsobhi@coppin.edu

How to cite this paper:, Ghann, W., Sobhi, H., Kang, H., Chavez-Gil, T., Nesbitt, F. and Uddin, J. (2017) Synthesis and Characterization of Free and Copper (II) Complex of N,N'-*Bis*(Salicylidene)Ethylenediamine for Application in Dye Sensitized Solar Cells. *Journal of Materials Science and Chemical Engineering*, **5**, 46-66.
https://doi.org/10.4236/msce.2017.56005

Received: May 10, 2017
Accepted: June 26, 2017
Published: June 29, 2017

Abstract

Dye sensitized solar cell represents a promising method for the conversion of solar energy to electric energy. In the present work free N,N'-*bis*(salicylidene)ethylenediamine and its copper (II) complex were synthesized, characterized, and investigated for use as dye sensitizers in the fabrication of dye sensitized solar cells. The dyes were characterized using UV-Vis, Steady State Florescence, and Fluorescence Lifetime, Thermogravimetric Analysis, Differential Scanning Calorimetry, and Cyclic Voltammetry. The thermogravimetric analyses of the ligand and the ligand Copper complex demonstrate the stabilizing effect of the copper ion on the ligand complex. Additionally, the copper ion is shown to stabilize the structure, as evidenced by the 150˚C increase in the extrapolated onset temperature of the decomposition event. The ligand copper complex is further stabilized by the presence of the copper, which is determined by the 6.34% residue that remained at the end of the thermogravimetric analysis, compared with 0% residue when applying the same condition for the ligand without copper. The current-voltage characteristics of the cells and the electrochemical impedance were determined. The photovoltaic performance of the solar cell devices fabricated using N,N'-*bis*(salicylidene) ethylenediamine dye was found to be slightly better than those produced from the copper complex. The solar to electric power efficiency of the ligand-based dye sensitized solar cell was 0.14% and that of the copper complex was found to 0.12%. Although the difference in the cell efficiency is quite small, it is obvious that the insertion of Copper into the ligand did not enhance the perfor-

mance of the solar cells. The photocurrent-photovoltage results are consistent with the absorption spectra that showed a more prominent band for the ligand. The free hydroxyl groups, present in the ligand but absent from the copper complex owing to their coordination with the copper metal, could be responsible for the difference in the performance of the devices. The hydroxyl groups get attached to the TiO_2 and facilitate the transfer of electrons.

Keywords

DSSC, Copper, N,N'-*Bis*(Salicylidene)Ethylenediamine, Dye, Titanium Dioxide

1. Introduction

Imines are uncharged compounds which contain a carbon-nitrogen double bond. Molecules of this type are used as synthetic intermediates, and they are of interest as biologically important molecules [1] [2] [3]. For example, imines play an important role in the chemistry of vision and in amino acid metabolism [4]. Imines also function as Lewis bases in coordination to metal ions. Imines are formed by condensation of a carbonyl compound with a primary amine. The synthesis and characterizations of imines are well documented in literature [5]. Imines are useful in so many applications. They are very important for transition metal based catalytic reactions such as epoxidation of olefins, lactide polymerization, and hydroxylation. [5] Some investigators have reported the synthesis and use of N,N'-*bis*(salicylidene)ethylenediamine zinc(II) iodide as an electrolyte for dye sensitized solar cells (DSSCs) [6]. We were interested in the possible use of N,N'-*bis*(salicylidene)ethylenediamine as photosensitizer for dye sensitized solar cells owing to their absorption characteristics.

Dye sensitized solar cells are low-cost and easily fabricated type of photovoltaic devices which were first developed by Michael Gratzel [7]. There has been an exponential growth in research and an increase in the number of publications focused on the optimization and large-scale production of dye sensitized solar cells [8]-[14]. In DSSC, dye molecules adsorbed onto mesoporous titanium dioxide absorb incident light and move to the excited state where an electron is transferred into the conduction band of the titanium dioxide semiconductor. The electron is subsequently transported through the titanium diode film through an external circuit to the cathode [13]. The TiO_2 has a large surface area that supports a great number of dye molecules and thus increase the amount of energy absorbed [15] [16] [17] [18]. The TiO_2 also receives electrons ejected from the dye and facilitates its transportation to an external circuit. Most of the dyes that have been used as sensitizers in the fabrication of dye sensitized solar cells are ruthenium (II) complexes [11] [19] [20] [21] [22]. We have carried out studies on the fabrication of dye sensitized solar cells using natural dyes [14] [23] [24] [25] and other synthetic dyes such as porphyrins, and phtalocyanine

[26] [27] [28] [29] [30]. The synthesis, spectral, electrochemical, and photovoltaic properties of N,N'-*bis*(salicylidene)ethylenediamine (ligand) and its copper (II) complex (ligand Cu(II)) are discussed in the present work.

2. Experimental Section

2.1. Materials

Titanium dioxide powder (Degussa P25) was purchased from the institute of chemical education. Fluorine tin oxide (FTO) conducting glass slides were purchased from Harford glass company, Hartford City, Indiana. Sodium Hydroxide (NaOH), acetone (C_3H_6O), ethanol (C_2H_5OH), and acetic acid (CH_3COOH) were purchased from Sigma-Aldrich and were used without further purification. Graphite used in making cathode slides was purchased from TED PELLA, INC. Steady-state absorption spectra of dyes in solution were acquired using UV-3600 Plus from Shimadzu. Steady-state fluorescence spectra were recorded on the fluorescence Nanolog Spectrofluorometer System from Horiba Scientific (FL3-22 iHR, Nanolog). ATR spectra were obtained with a Thermo Nicolet iS50 FTIR. Electrochemistry determinations were collected in DMF solutions on a Princeton Applied Research VersaSTAT-3 potentiostate using a three-electrode cell unit. Transmission Electron Microscopy (TEM) images were acquired on JEM-1400 Plus (JEOL USA, Peabody, Massachusetts). The images were viewed using Digital Micrograph software (Gatan, Inc., Pleasanton, CA). HOMO and LUMO calculations were carried out using Spartan'16 software from Wavefunction, Inc., Irvine, CA, USA. TiO_2 paste was printed on FTO glass using WS-650 Series Spin Processor from Laurell Technologies Corporation.

2.2. Synthesis of Ligand

The ligand was synthesized according to the synthetic route displayed in **Figure 1**. First, salicylaldehyde (20 mmol) was dissolved in 15 mL of methanol in a 25 mL round bottom flask. In a separate 25 ml flask, ethylene diamine (10 mmol) was dissolved in 10 ml methanol. The salicylaldehyde solution was added dropwise to the ethylene diamine solution while stirring (400 rpm) at room temperature for a period of 15 minutes. The precipitation of the product was observed by the formation of yellow precipitate, and was completed within 15 minutes. Afterwards the reaction flask was placed in an ice water bath for 10 minutes followed by the filtration of the reaction mixture using a Hirsh funnel. The precipitate was washed with ice cold methanol and air dried to form light yellow flakes. The yield was 82.7% and the melting point was 126.8˚C. ^{1}H NMR ($CDCl_3$) δ/ppm: 13.24 (s, 2H), 8.38 (s, 2H), 7.33 - 7.24 (m, 4H) 6.86 - 6.97 (m, 4H), 3.96 (s, 4H). ^{13}C NMR ($CDCl_3$) δ/ppm: 166.47, 160.95, 132.36, 131.45, 118.65, 118.59, 116.91, 59.71.

2.3. Synthesis of Ligand Cu (II)

The ligand Cu (II) was synthesized according to published protocol with little

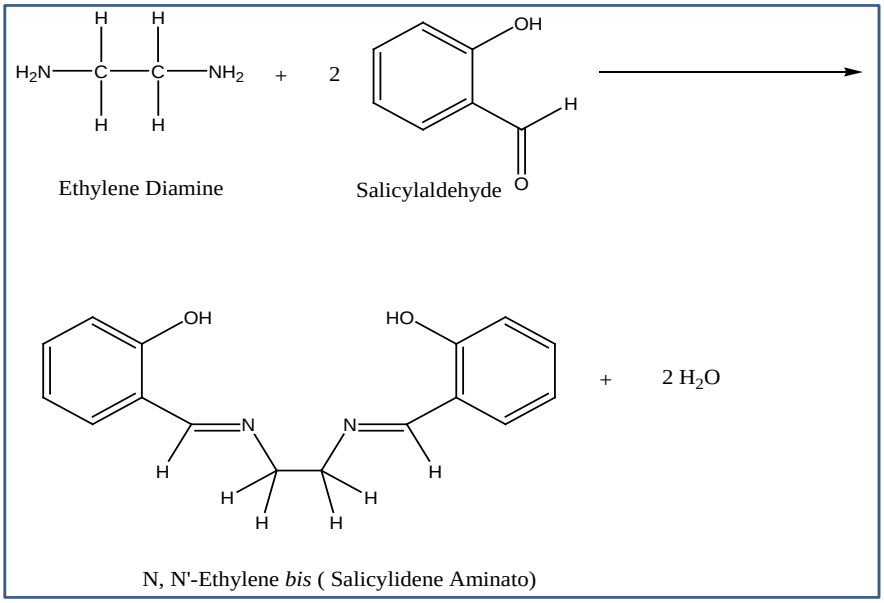

Figure 1. Synthetic route to N,N'-*bis*(salicylidene)ethylenediamine (denoted ligand).

modification as displayed in **Figure 2** [6] [31] [32] [33]. Copper (II) acetate monohydrate dissolved in hot methanol was added dropwise to a stirred hot solution of the ligand (0.5 mmol) in the same solvent. Upon completion, the reaction mixture was cooled to room temperature, filtered, washed thoroughly with water and methanol and air dried. The product collected consisted of dark greenflakes of ligand Cu (II), with percent yield of 65.7%. ^{1}H NMR ($CDCl_3$) δ/ppm: 7.45 (s, 2H), 7.33 - 7.24 (m, 4H) 7.06 (t, 2H) 6.57 (t, 2H), 3.51 (s, 4H). ^{13}C NMR ($CDCl_3$) δ/ppm: 164.82, 161.79, 133.92, 132.24, 121.70, 119.98, 115.06, 77.35, 77.24, 77.03, 76.72, 58.44.

2.4. Fluorescence Lifetime Measurements

The dye samples were dissolved in 3 mL of ethanol for fluorescence lifetime measurement. To prevent inner filter effect, absorption measurements were carried out to ensure the absorbance of the dyes was less or equal to 0.15 absorbance unit. Fluorescence decays were measured using Horiba deltaflex fluorescence lifetime system using the time-correlated single-photon counting (TCSPC) technique with the PPD-850 picosecond photon detection module. The excitation source was 340 nm light-emitting diodes (Delta LED).

2.5. Thermal Analysis Experiments

The synthesized ligand and ligand Cu (II) were tested for their thermal stability using the Differential scanning calorimetry (Discovery DSC, TA Instruments-Waters LLC, New Castle, DE)/Conventional 170˚C oven method. Two samples each of the ligand and the ligand Cu (II) were carefully weighed into four pre-weighed pans and placed in an infrared isotherm vacuum oven. The samples weights were determined to be within the range of 1.5 to 5.0 mg. The Differential scanning calorimetry (DSC) analysis was carried out in three cycles. In cycle I,

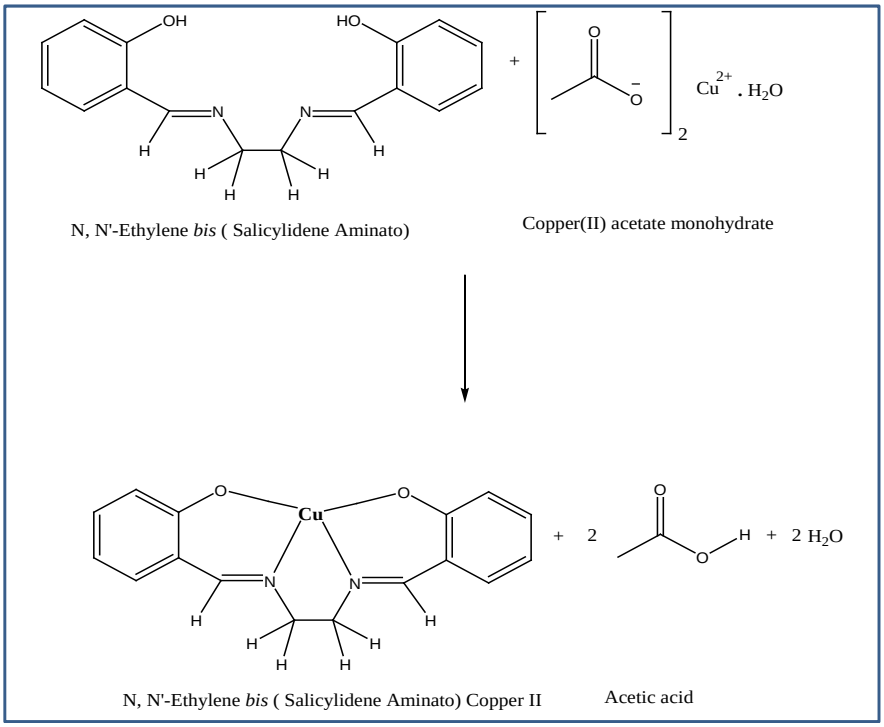

Figure 2. Synthetic route to N,N'-*bis*(salicylidene)ethylenediamine copper (II) (denoted ligand Cu (II)).

the oven was first equilibrated at 25˚C, and ramp to 170˚C at a rate of 10˚C/min; this was followed by a second oven ramp to 170˚C at a rate of 10˚C/min in cycle II and final oven ramp to 170˚C at a rate of 10˚C/min in cycle III. The pans containing sample were subsequently left in the oven for 2 h at 15 kPa vacuum and immediately placed in desiccator under vacuum for another hour. Following this, the pans were removed from the desiccator and their weights determined.

2.6. Thermogravimetric Analysis

The Thermogravimetric Analyzer Model 55 (Discovery TGA, TA Instruments-Waters LLC, and New Castle, DE) was used to measure the thermal stability of both bound and unbound N, N-Ethylene *bis*(Salicylidene aminato) ligand, and the ligand Cu (II). The samples were prepared by placing one drop of the material on to a pre-tared platinum TGA pan. The pan was placed onto the autoloading mechanism of the TGA, and an automated loading sequence was initiated. The sample was then placed into a furnace which heats the sample, while simultaneously measuring the mass of the sample every 0.5 s. The TG experimental conditions were Ramp 10˚C per minute to 700˚C in nitrogen gas. All TG experiments were performed using 30 - 40 mg of each sample.

2.7. Cyclic Voltammetry

Electrochemical characterization of ligand and Cu (II) complexes were carried out in organic solutions using a one-compartment three-electrode cell equipped with a platinum disk working electrode (1.6 mm diameter) from Basi-Analytical

Instruments, a platinum wire as auxiliary electrode, and $Ag/AgNO_3$ (0.10 M, in acetonitrile) as reference electrode. The working electrode was polished first using 0.30 μm followed by 0.05 μm alumina polish (BASi). The supporting electrolyte was 0.1 M tetrabutylammonium perchlorate (Bu_4NClO_4) dissolved in DMF. All potentials were converted to the SHE scale by adding 0.50 V to the experimental data [34]. The cyclic voltammetry were carried out on a Princeton Applied Research VersaSTAT-3 potentiostate with samples degassed under a nitrogen flow before each scan.

2.8. Fabrication of Solar Cell

The solar cell devices were prepared according to a modified protocol [35] [36] [37]. In brief, the photoanode was prepared by depositing a thin film of TiO_2 on the conductive side of a fluorine doped tin oxide (FTO) glass using a spin coater and heating the film at 380˚C for 2 hours. The TiO_2 covered FTO glass was then immersed in a freshly prepared solution of the dye for a period of four hours, rinsed with ethanol and air dried. The counter electrode (cathode) was prepared by painting FTO glass with colloidal graphite. The dye-sensitized electrode and the carbon electrode were assembled to form a solar cell sandwiched with a redox (I^-/I^{3-}) electrolyte solution.

2.9. Photovoltaic Properties Measurement

The energy efficiencies of the fabricated DSSCs were measured using 150 W fully reflective solar simulator with a standard illumination with air-mass 1.5 global filter (AM 1.5 G) having an irradiance corresponding to 1 sun (100 mW/cm^2) purchased from Sciencetech Inc., London, Ontario, Canada and Reference 600 Potentiostat/Galvanostat/ZRA from Gamry Instruments (734 Louis Drive, Warminster, PA 18974). The tested solar cells were masked to an area of 5 cm^2. Each cell performance value was taken as the average of three independent samples. The solar energy to electricity conversion efficiency (η) was calculated based on the equation:

$$\eta = FF \times I_{sc} \times V_{oc} \quad (1)$$

where FF is the fill factor, I_{sc} is the short-circuit photocurrent density ($mA \cdot cm^{-2}$), and V_{oc} is the open-circuit voltage (V) as listed in **Table 3**.

3. Results and Discussion

3.1. UV-Vis Absorption Studies

The optical properties of the dyes were investigated using UV-Vis spectrometry. The overall performance of a DSSC depends on the light harvesting capability of the dye sensitizer [15] [38] [39]. As illustrated in **Figure 3**, two broad bands were observed in the spectra of the ligand occurring at 255 nm and 318 nm and assigned to π - π^* transition [6]. An additional band at 406 nm accounting for n - π^* transition is less prominent compared to the corresponding peak of the ligand Cu (II). The first broad band of ligand Cu (II) is similar to that of the li-

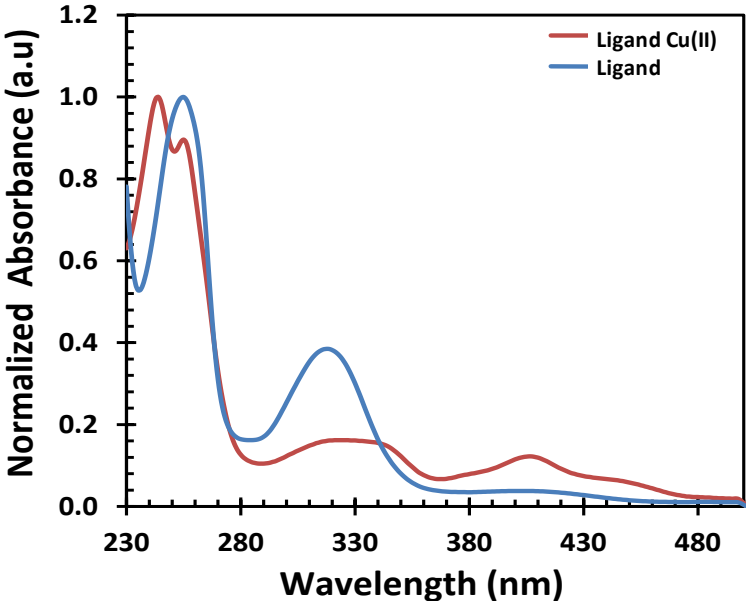

Figure 3. UV-Vis absorption spectra of ligand and ligand Cu (II) in ethanol at a concentration of 1.0×10^{-4} mol·L^{-1}.

gand except the band is red shifted and has a slight shoulder. The absorption band of the ligand Cu (II) at 330 nm is red shifted to that of the ligand (318 nm), a direct result of the coordination of the copper to the ligand which lowers the π^* orbital of the ligand and consequently the energy of the π - π^* transition.

3.2. Steady State Fluorescence Studies

Fluorescence spectra of the dyes employed in the fabrication of the DSSC were obtained in order to examine their emission characteristics. The fluorescence spectra of the ligand and ligand Cu (II) is displayed in **Figure 4**. The measurement was carried out with an exciting light (λexc) of 320 nm. The emission patterns of both dyes were different, resembling that of the absorption in which the band of the ligand was very high. There is a slight blue shift in the peak of ligand Cu (II) with respect to ligand at the peak around 435 nm as well as at 340 nm. The huge peak of the ligand at 435 with respect to the ligand Cu (II) is a reflection of the amount of energy first absorbed by the ligand and how it might be a better candidate as dye for dye sensitized solar cells.

3.3. Fluorescence Lifetime Measurements

The Lifetimes of the ligand and ligand Cu (II) were determined by time-correlated single photon counting in ethanol as illustrated in **Figure 5** and **Table 1**. The measurements were carried out to evaluate the impact of these lifetime decay parameters on the performance of dye sensitized solar cells. The fluorescence decay profiles were analyzed by two-exponential fit giving two components with lifetimes of 2.17 ns and 9.2 ns for the free ligand and 5.3 ns and 15.5 ns for the ligand Cu (II). A ludox sample was used to generate an instrument response before lifetime of any of the samples was measured. The ludox sample which

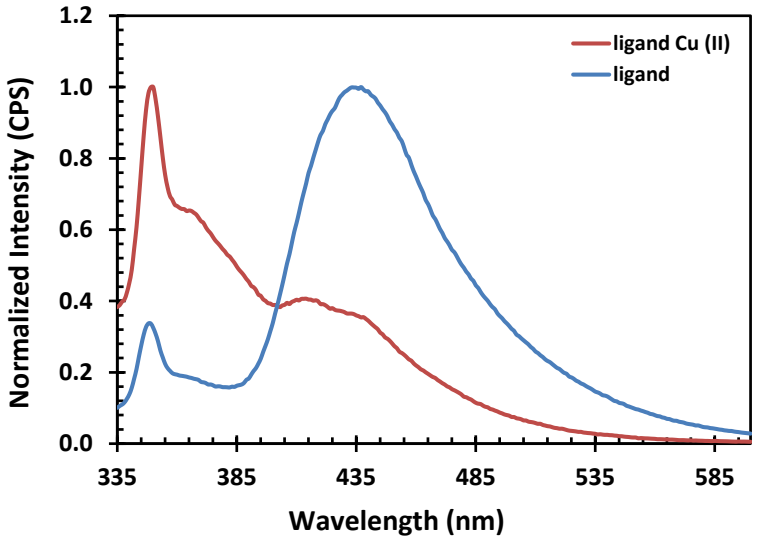

Figure 4. Emission spectra of ligand and ligand Cu (II) in ethanol at a concentration of 1.0×10^{-4} mol·L^{-1}.

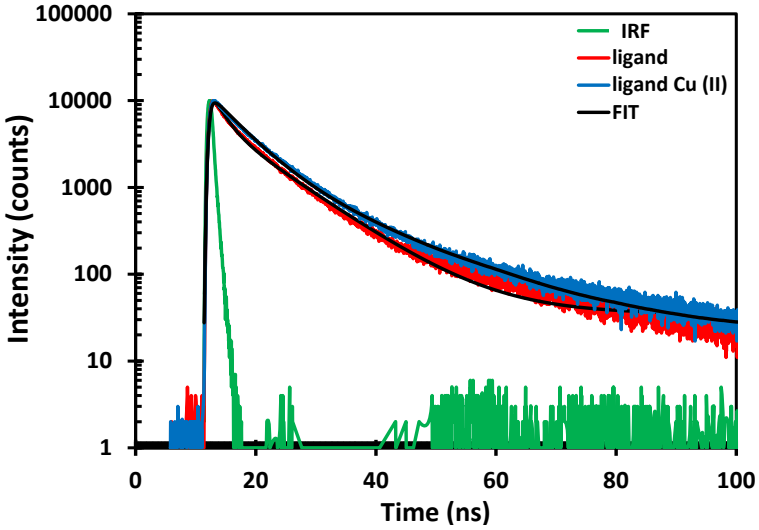

Figure 5. Fluorescence decay curves measured by time-correlated single-photon counting (TCSPC) technique for ligand Cu (II) and ligand, instrument response, and FIT.

Table 1. Fluorescence lifetime measurement of ligand and ligand Cu (II).

Sample	τ_1	τ_2	χ^2
Ligand Cu (II)	5.3 ns	15.5 ns	2.95
Ligand	2.17 ns	9.2 ns	3.79

served as the prompt was a scattering solution which did not contain any fluorophore.

3.4. FTIR Studies

IR studies were conducted on the ligand and ligand Cu (II) samples to examine changes in the spectra before and after the incorporation of copper in order to

understand the vibrational modes of the dyes and the phase transition due to occur when the electronic environment change upon attachment to TiO_2 nanoparticles. The spectra of ligand and ligand Cu (II) were measured in the solid state in KBr disks within the range 4000 - 400 cm^{-1} as illustrated in Figure 6. An interesting observation in this study was that the stretching intensities were increased when copper was introduced into the molecule. The characteristic peak of the imines (C=N−) and their metal complexes are known to occur in the 1670 - 1500 cm^{-1} region. This imine peak was observed in the spectra of the ligand as strong doublet at 1680 and 1560 cm^{-1} as well as in the Cu (II) complex as illustrated in Figure 6. The C-C-H stretching for the ligand is observed in the region of 3200 - 2700 cm^{-1} and is assigned to intramolecular hydrogen bonds [6]. After copper's coordination, the IR spectra is substantially modified due to the breaking of intramolecular hydrogen bonds and its substitution for the metal-ligand interaction which results in new stretching's at 1576 cm^{-1} $_{as-sym\nu}$(Cu-N=C-), (480$_{\nu}$(Cu-O), and symmetric 420 $_{sym\nu}$(Cu-N) cm^{-1}, with a deep modification on the two stretching's observed at 860 and 755 cm^{-1} for the ligand [40] [41]

3.5. Fundamental Thermal Analysis of the ligand

The DSC analyses of the materials each show a primary endotherm, with the pure ligand exhibiting a melting onset near 125˚C and a melting enthalpy of 124.16 J/g. Introduction of the copper into the matrix disrupts the crystallinity and thermal stability of the ligand, as evidenced by a dramatic decrease in the melting enthalpy (8.2 J/g) as well as a concomitant 13˚C decrease in the melting temperature onset.

3.6. Thermogravimetric Analysis

Thermogravimetric analyses of the ligand and ligand Cu (II) illustrate the stabi-

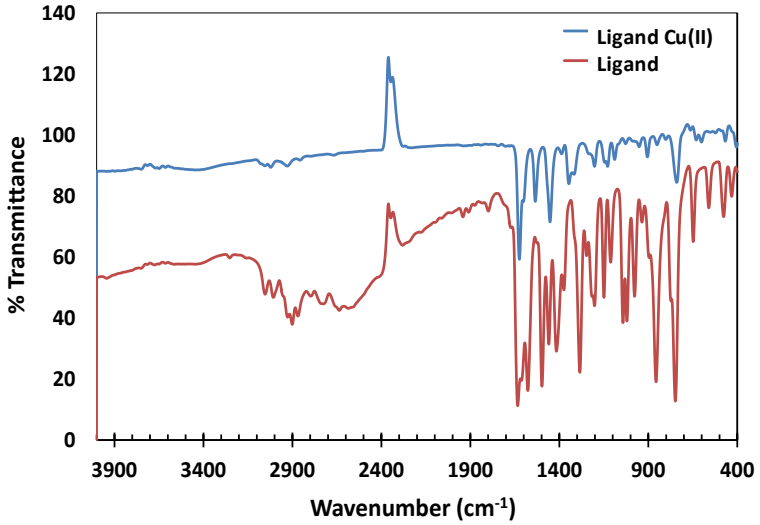

Figure 6. FT-IR spectra of ligand (blue) ligand Cu (II) (red) in the range 4000 - 400 cm^{-1}.

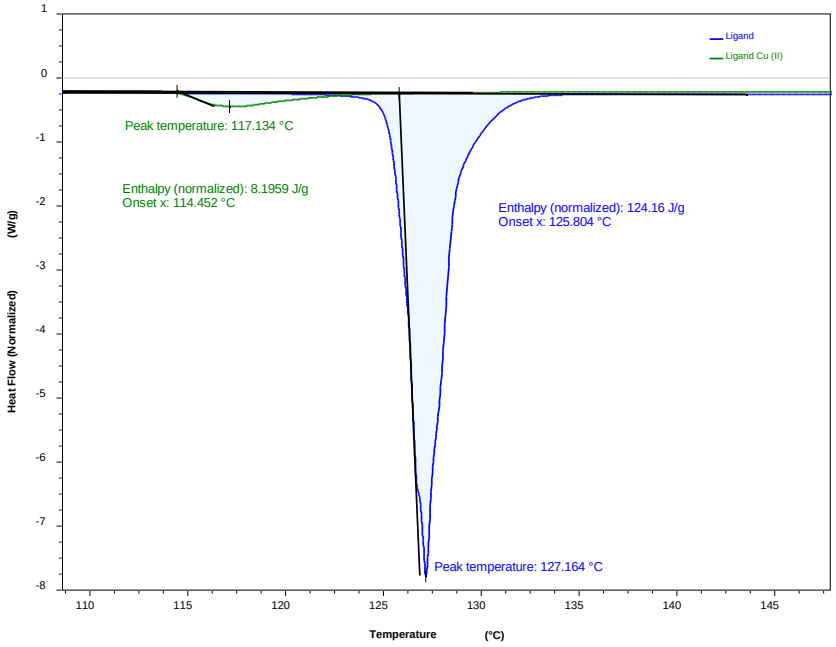

Figure 7. Differential Scanning Calorimetry—DSC of ligand (blue) and Cu (II) complex (green).

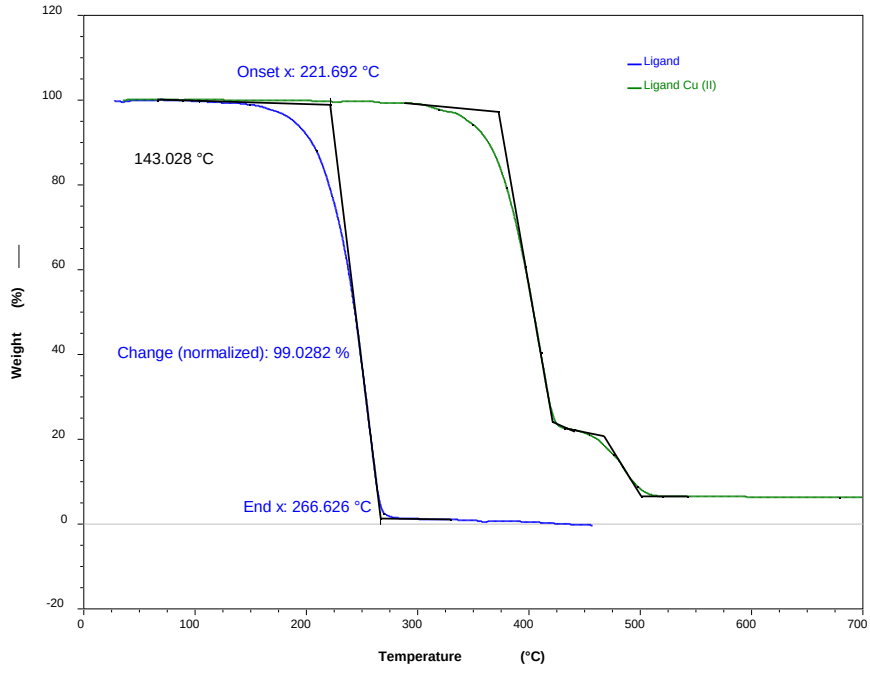

Figure 8. Thermogravimetric Analysis—TGA of ligand (blue) and Cu (II) complex (green).

lizing effect of the copper ion on the ligand complex. The pure ligand shows a primary decomposition starting near 143˚C and a singular decomposition event which is completed near 225˚C. Addition of the copper ion is shown to stabilize the structure, as evidenced by the 150˚C increase in the extrapolated onset temperature of the decomposition event. In addition, the bimodal decomposition

profile suggests an intermediary phase which is further stabilized by the presence of the copper ion. The 6% residue analysis is attributed to reduced copper.

3.7. Transmission Electron Microscopy Imaging

To confirm the adsorption of the ligand and ligand Cu (II) dyes on the TiO_2 nanoparticles, high-resolution images were taken via transmission electron microscopy. To take the TEM images ethyl alcohol solutions of the ligand and ligand Cu(II) were used to make colloidal suspension with TiO2 power. A drop of each suspension was placed on a TEM grid and allowed to dry in a hood overnight. As shown in Figure 9, the sizes of the anatase TiO_2 nanoparticles were found to be within the range of 20 - 25 nm. The sizes of ligand molecules seen as spherical particles around the TiO_2 nanoparticles were determined to be within the range of 1 - 3 nm (Figure 9(a)), (the arrows in the images are guide to the dyes). The free ligands are able to bind to the TiO_2, whereas the ligand with copper ions barely sits on the TiO_2 nanoparticles (Figure 9(b)). The binding between the ligand dye and the TiO_2 nanoparticles results from the deprotonation of hydroxyl groups from the ligand. However, since the ligand Cu (II) does not have the hydroxyl groups due to the binding with the copper, many ligand dyes are observed in the spaces in-between TiO_2 nanoparticles.

3.8. Cyclic Voltammetry

The cyclic voltammogram of ligand in concentration of 1.2 μM ($NbuN_4ClO_4$/DMF) solution is illustrated in Figure 10(a), and summarized in Table 2. The CV of ligand recorded at scan rate, υ, of 50 $mV \cdot s^{-1}$ at 25˚C is characterized by two irreversible redox waves. A first irreversible, sharp and low-current wave with peak potential at $E_{1/2}$ = 0.54 V versus SHE was observed, and a second strong irreversible wave with peak potential at $E_{1/2}$ = 1.42 V versus SHE characterize the ligand's redox reaction. These two electrochemical half-cell ($E_{1/2}$) peak potentials correspond to the transfer of one electron from each side of the substrate that becomes irreversible perhaps to secondary reactions, which leads to electrochemically inactive species. This hypothesis is related with the open chain geometry of substrate that contribute to its electrochemistry irreversibility due to the second electron evolved in the oxidation process experience a synergistic

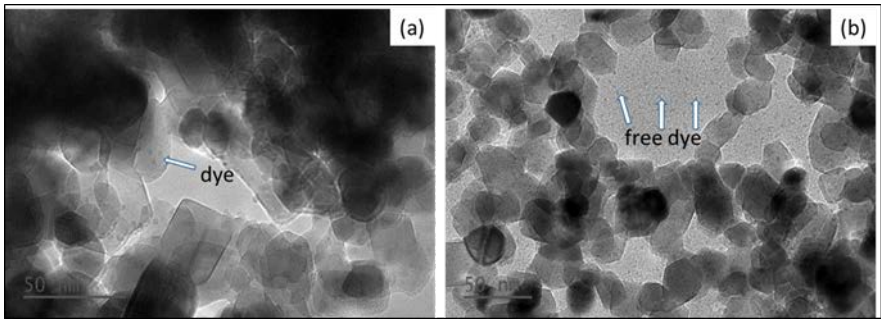

Figure 9. High-resolution TEM images of the ligand/TiO_2 and ligand Cu (II)/TiO_2 nanoparticle: (a) ligand/TiO_2, and (b) ligand Cu (II)/TiO_2.

input on the formation of inactive species generated during the first oxidation reaction as shows the enhanced amperometric values (see Table 2) for the second oxidation peak potential and the total decay of the reversible process. In addition, a deeply decreasing on the oxidation signal was observed after the first

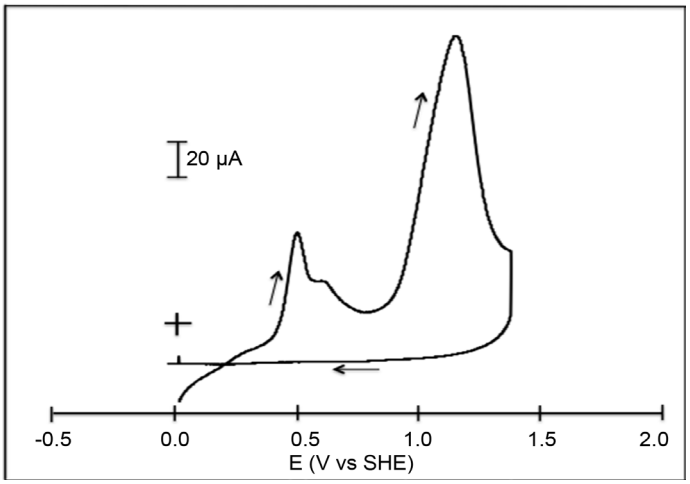

(a)

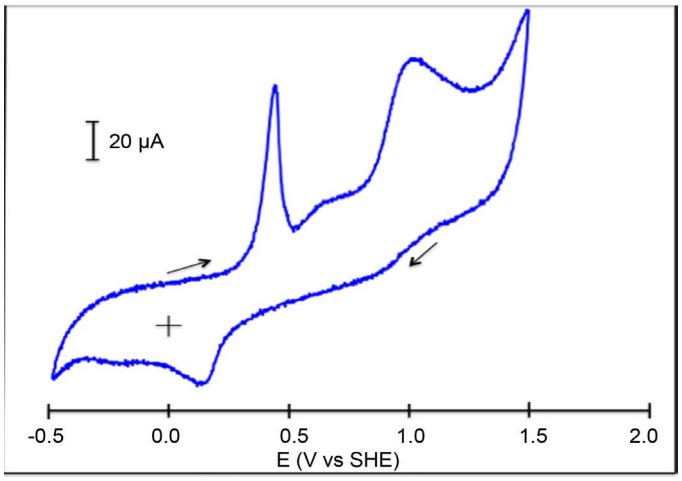

(b)

Figure 10. Cyclic voltammograms of ligand (a), and ligand Cu(II) (b) at 1.2 µM concentration in TBAP 0.1 M (DMF). Scan rates were 50 mV·s^{-1}, and 10 mV·s^{-1} (25˚C), respectively.

Table 2. Redox potentials of ligand and Cu (II) complex.

Compound	E_{pa} (mV)[a]	E_{pc} (mV)	Assignment
L	0.54	---	L 0/+
	1.42	---	L +/-
Cu-L	0.48		Cu^{II}/Cu^{III}
Cu-L		0.21	Cu^{III}/Cu^{II}
Cu-L	1.01		L_{coord} +/-

[a]Potentials reported versus the SHE reference electrode in acetonitrile with concentration ranged from 1.0-1.2 µM in 0.1 M of $[Nbu^{n}_{4}][X]$ (X = ClO_4) as supporting electrolyte. Working electrode Pt.

scan with a subsequently film deposition on the work's electrode surface, which leads to a complete color change in the solution as proof of dye decomposition during an electrochemistry induced electrons transfer reaction.

Upon coordination with metallic ions, the chromophore makes its oxidation reaction easier with its redox potentials shifted towards lower potential values. The results of our experiments show that ligand as well as the Cu (II) complex undergoes a one electron transfer reaction with peak potential, $E_{1/2}$ = 0.48 V and $E_{1/2}$ = 0.21 V versus SHE in DMF (**Figure 10(b)**) attributed to the Cu^{III}/Cu^{II} couple redox process [42] in a quasi-reversible one electron transfer as indicated by the peak current ratio, i_a/i_c which is close to unity (herein, 1.1) at the scan rates investigated (10 - 50 $mV{\cdot}s^{-1}$). The peak separation between the anodic and cathodic peak potentials, E_{pa} - E_{pc}, shows to be close to 0.53 V (one electron transfer), which is attributed to a reversible electrochemistry one electron transfer. These values are in agreement with the theoretical value of 59 mV for a one-electron transfer reaction, that for a reversible process the peak width is given by the difference in the thermodynamic relationship:

$$E_{p/2} - E_p = 2.2\left[\frac{RT}{nF}\right] \tag{2}$$

where $E_{p/2}$ is the half-peak potential at the half value of the peak current, E_p, is the peak potential, F is the Faraday constant and n is the number of electrons transferred during the reaction. The presence of copper ions coordinated as bis-(oxo and imine) units, makes the oxidation reaction of this complex easier than the ligand alone with the redox potentials shifted towards lower values as depicted in **Figure 10(b)**.

The redox reaction was slightly symmetric for one electron donating and withdrawing in the Cu (II) complex which showed a quasi-reversible behavior indicating that the material is moderately air stable. Some broadening occurred, however, due to uncompensated resistance. Thus, the diiminosalicylate macrocycle makes the electron transfer easier to oxidation due to the presence of metal ions in the complex instead of the irreversibility process observed on the single chromophore. One can conclude from these experiments, that the ligand alone is an electron donor/withdrawing chromophore and then, its bond stabilization energy is decreased after coordination by turning easier its redox reactions [43]. This assumption is evidenced by the low shift potential that was found at $E_{1/2}$ = 1.01 V in the complex, whereas the same one electron transfer occurred at high potentials such as $E_{1/2}$ = 1.42 V on the free subtract. Therefore, the net change in the coordination energy between the ligand and the complex was found to be, $\Delta E_{1/2}$ = 0.41 V versus SHE electrode.

3.9. Current-Voltage Characteristics

The photocurrent-photovoltage (I-V) performance of the ligand and ligand Cu (II) dye sensitized solar cell devices were assessed under simulated sunlight at AM 1.5 (100 $mW{\cdot}cm^{-2}$) and is displayed in **Figure 11**. The parameters related to

the cell performance such as the short circuit current (I_{sc}), open circuit voltage (V_{oc}), fill factor (FF) and Efficiency (η) are displayed in Table 3. The dye sensitized solar cell fabricated with the free ligand exhibited a slightly higher performance: I_{sc} = 0.88 mA/cm^2, V_{oc} = 0.49 V, FF = 0.32, η = 0.14, compared to that of the copper complex of the ligand which had efficiency (η) of 0.12% with I_{sc} = 1.22 mA/cm^2, V_{oc} = 0.28 V, FF = 0.37. It was determined through the thermogravimeteric analysis that the copper complex of the ligand was more stable than the free ligand. However, the performance of dye sensitized solar cells is dependent on the kind of interaction between the dye and the nanocrystalline titanium dioxide electrode. The higher performance of the device fabricated with the free ligand could be attributed to the presence of the hydroxyl groups that are known to bind to the TiO_2 nanoparticles facilitating the transfer of electrons.

3.10. Electrochemical Impedance Spectroscopy

Solar cells fabricated using ligand and ligand Cu (II) were tested for kinetics and energetics of charge transport and recombination. Impedance measurements were carried out at frequencies between 0 and 100 KHz. Figure 12(a) shows the Nyquist plots and Figure 12(b), the Bode plot of the two samples which were

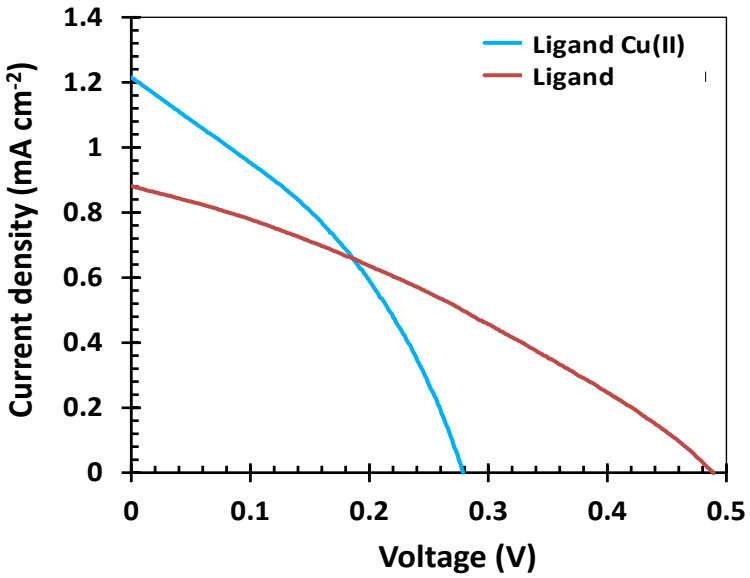

Figure 11. Photocurrent-voltage characteristics of dye sensitized solar cell devices under illumination of 100 mW/cm^2 simulated AM 1.5 sunlight. Devices fabricated using ligand Cu (II) and ligand.

Table 3. Current and voltage characteristics for the dye sensitized solar cell fabricated using ligand and ligand Cu (II).

DYE	Isc	Voc	Imp	Vmp	Fill Factor	Efficiency
	(mA/cm^2)	(V)	(mA/cm^2)	(V)		(%)
Ligand	0.88	0.49	0.54	0.26	0.32	0.14
Ligand Cu (II)	1.22	0.28	0.74	0.17	0.37	0.12

investigated. The results seen here is consistent to the current and voltage characteristics of the solar cells. As shown in the Nyquist plot (Figure 12(a)) a larger circle is observed for ligand Cu (II) and this could be as a result of the recombination of the injected electron with the electrolyte by a backward transfer in lieu of the electron traveling through TiO_2 mesoporous film. The bode plot of the ligand and ligand Cu (II) displayed in Figure 12(b) show results somewhat related to the information obtained from the Nyquist data. The Bode plot offer information on the lifetime of the injected electron. The time the electron travel from the dye to the titanium dioxide can be deduced from the position of the frequency peak. Shift to lower frequency is indicative of long electron lifetime or recombination lifetime. The Bode plots show that the ligand will have a longer lifetime and lower transport resistance.

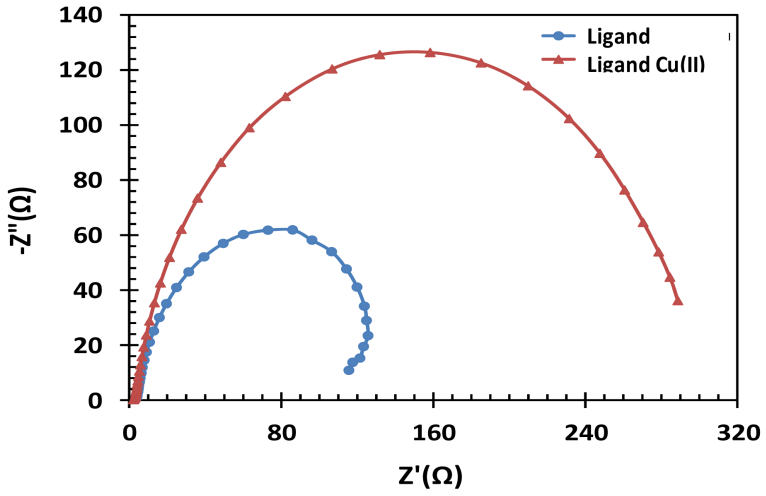

(a)

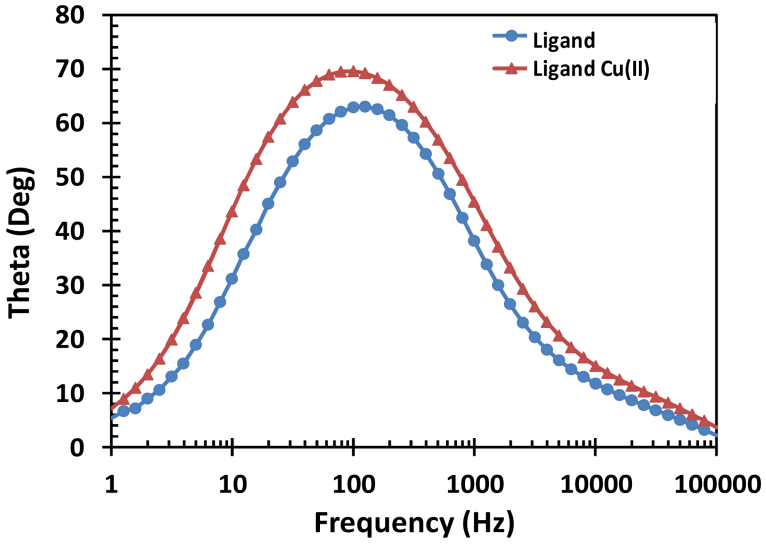

(b)

Figure 12. Impedance studies of the fabricated devices: (a) Nyquist plots of the dye sensitized solar cells fabricated using ligand and ligand Cu (II); (b) Bode plots of dye sensitized solar cells fabricated using ligand and ligand Cu (II).

3.11. Density Functional Calculations for N,N'-Ethylene *bis*(Salicylidene Aminato) and It Copper Complex

Density functional calculations were used to optimize the geometry of the ligand and ligand Cu (II) using the software Spartan 16 from Wavefunction. All geometries were computed using the ωB97X-D density functional theory method. Geometry optimization was performed using 6 - 31G* basis set. These calculations were used to compute the highest occupied molecular orbital (HOMO) and the lowest unoccupied molecular orbital (LUMO) energies of the ligand as well as the highest occupied molecular orbitals (aHOMO), (bHOMO) and the lowest unoccupied molecular orbital (aLUMO), (bLUMO) energies of ligand Cu (II). The calculations gave a result for the HOMO and LUMO of the ligand as −7.82 eV and 0.51 eV, respectively.The difference in the HOMO and LUMO, which is the band gap of the ligand, was found to be 8.33 eV. The LUMO and HOMO surfaces and orbital energy diagrams of the ligand are shown in **Figure 13(a)** and **Figure 13(b)**, respectively. In **Figure 13(a)** and **Figure 13(b)**, the blue and red regions represent positive and negative values of the orbitals, respectively.

The calculations gave the same result for the aHOMO and bHOMO of −14.6 eV but the results for the aLUMO and bLUMO of −9.5 eV and −9.9 eV, respectively. The difference in the aHOMO and aLUMO which is the band gap-a was 5.1 eV. The difference in the bHOMO and bLUMO which is the band gap-b was 4.7 eV. The aHOMO and aLUMO surfaces and orbital energy diagrams are shown in **Figure 13(c)** and **Figure 13(d)**, respectively. The bLUMO and bHOMO surfaces and orbital energy diagrams are shown in **Figure 13(e)** and **Figure 13(f)**, respectively. In **Figure 13(c)-(f)**, the blue and red regions represent positive and negative values of the orbitals respectively.

Upon receiving photons from sunlight and other solar sources, dye molecules (S) adsorbed on the TiO_2 film gain energy and transition from the ground state or the highest occupied molecular orbital (HOMO) to an excited state or the lowest unoccupied molecular orbital (LUMO) state as displayed in **Figure 14**.

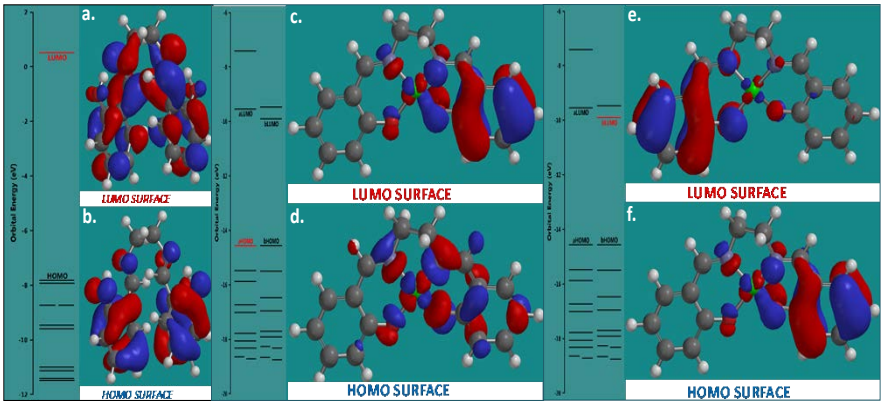

Figure 13. Surfaces and orbital energy diagrams of the ligand (a) LUMO; (b) Ligand Cu (II) square planar complex; (c) The aHOMO surface and orbital energy diagram; (d) The aLUMO surface and orbital energy diagrams; (e) The bHOMO surface and orbital energy diagrams; (f) The bLUMO surfaces and orbital energy diagrams.

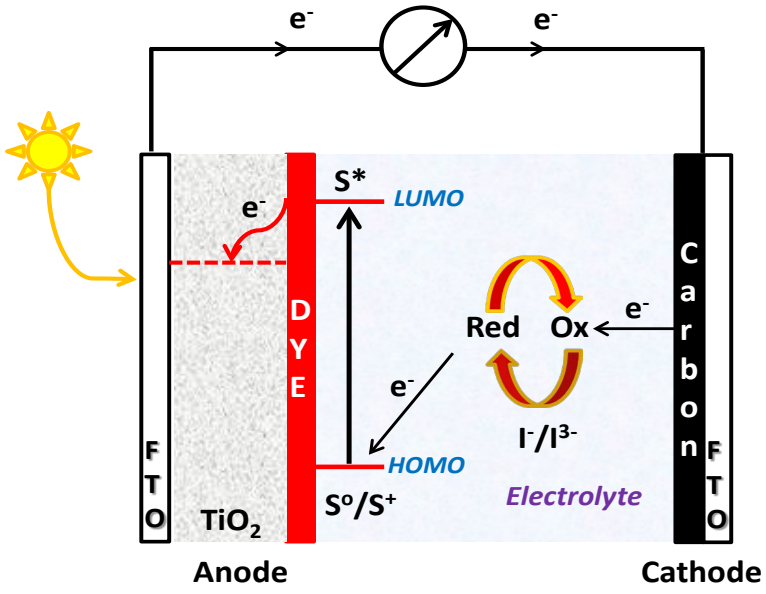

Figure 14. Generalized energy diagram of a dye sensitized solar cell

The photoexcited species (S^*) injects an electron into the conduction band of TiO_2 electrode and becomes oxidized (S^+). The electron deficient dye subsequently accepts an electron from the electrolyte (I^-) to restore the ground state of the dye (S). The injected electron travels through the nanocrystalline TiO_2 film to the conductive layer of the glass and subsequently through an external circuit to a load where the work done is delivered as electrical energy. The electron from the external load diffuses to the cathode where it gets transferred to the electrolyte (I_3^-), so the electrolyte system is regenerated.

4. Conclusion

We have synthesized a pair of Salicylidene aminato compounds, one with a copper metal and the other without a copper metal. The dyes were characterized using Nuclei Magnetic Resonance (NMR), Mass Spectrometry, Absorption Spectroscopy, Fluorescence Spectroscopy, and Transmission Electron Microscopy. The morphology as displayed in the imaging studies showed a good interaction between the dye and the nanocrystalline titanium dioxide film. The performance characteristics of the devices in terms of current-voltage and Impedance measurement showed the devices fabricated with the free ligand to have higher performance than those fabricated with the copper complex of the ligand. The solar-to-electric conversion efficiency of the device fabricated with the ligand was 0.14% whereas the efficiency of that of the metal complex was 0.12%. The photovoltaic result obtained is consistent with the UV-Vis measurement which presented a broader band in the absorption spectra of the ligand. Although the thermogravimetric analysis revealed that the incorporation of the copper metal enhanced the stability of the copper-ligand complex, the free hydroxyl groups on the ligand that enable the ligand to bind to the TiO_2 and thus facilitate electron transfer, are not present on the copper complex due to the

coordination of the metal to the ligand.

Acknowledgements

The work was financially supported by the University of Maryland System (Wilson E. Elkins Professorship), Constellation, an Exelon Company (E2-Energy to Educate grant program) and Dept of Education (SAFRA Title III Grant). The authors are also grateful to the Institution of Advancement, Coppin State University, for administrative help. The content is exclusively the responsibility of the authors and does not necessarily represent the official views of the funding agencies.

References

[1] Martin, S.F. (2009) Recent Applications of Imines as Key Intermediates in the Synthesis of Alkaloids and Novel Nitrogen Heterocycles. *Pure and Applied Chemistry*, **81**, 195-204.

[2] Wu, Y., Hu, L., Li, Z. and Deng, L. (2015) Catalytic Asymmetric Umpolung Reactions of Imines. *Nature*, **523**, 445-450. https://doi.org/10.1038/nature14617

[3] Qin, W., Long, S., Panunzio, M. and Biondi, S. (2013) Schiff Bases: A Short Survey on an Evergreen Chemistry Tool. *Molecules*, **18**, 12264-12289. https://doi.org/10.3390/molecules181012264

[4] Hallen, A., Jamie, J.F. and Cooper, A.J.L. (2014) Imine Reductases: A Comparison of Glutamate Dehydrogenase to Ketimine Reductases in the Brain. *Neurochemical Research*, **39**, 527-541. https://doi.org/10.1007/s11064-012-0964-1

[5] Layer, R.W. (1963) The Chemistry of Imines. *Chemical Reviews*, **63**, 489-510. https://doi.org/10.1021/cr60225a003

[6] Yang, S., Kou, H., Wang, H., Cheng, K. and Wang, J. (2010) Efficient Electrolyte of N,N'-Bis(Salicylidene)Ethylenediamine Zinc(II) Iodide in Dye-Sensitized Solar Cells. *New Journal of Chemistry*, **34**, 313-317. https://doi.org/10.1039/B9NJ00405J

[7] O'Regan, B. and Gratzel, M. (1991) A Low-Cost, High-Efficiency Solar Cell Based on Dye-Sensitized Colloidal TiO_2 Films. *Nature*, **353**, 737-740. https://doi.org/10.1038/353737a0

[8] Bella, F., Gerbaldi, C., Barolo, C. and Gratzel, M. (2015) Aqueous Dye-Sensitized Solar Cells. *Chemical Society Reviews*, **44**, 3431-3473. https://doi.org/10.1039/C4CS00456F

[9] Hagfeldt, A., Boschloo, G., Sun, L., Kloo, L. and Pettersson, H. (2010) Dye-Sensitized Solar Cells. *Chemical Reviews*, **110**, 6595-6663. https://doi.org/10.1021/cr900356p

[10] Hagfeldt, A. and Grätzel, M. (2000) Molecular Photovoltaics. *Accounts of Chemical Research*, **33**, 269-277. https://doi.org/10.1021/ar980112j

[11] Chen, C.Y., Wang, M., Li, J.Y., Pootrakulchote, N., Alibabaei, L., Ngoc-le, C.H., Decoppet, J.D., Tsai, J.H., Gratzel, C., Wu, C.G., Zakeeruddin, S.M. and Gratzel, M. (2009) Highly Efficient Light-Harvesting Ruthenium Sensitizer for Thin-Film Dye-Sensitized Solar Cells. *ACS Nano*, **3**, 3103-3109. https://doi.org/10.1021/nn900756s

[12] Gratzel, M. (2003) Dye-Sensitized Solar Cells. *Journal of Photochemistry and Photobiology C*, **4**, 145-153.

[13] Wei, D. (2010) Dye Sensitized Solar Cells. *International Journal of Molecular*

Sciences, **11**, 1103-1113. https://doi.org/10.3390/ijms11031103

[14] Shalini, S., Balasundara Prabhu, R., Prasanna, S., Mallick, T.K. and Senthilarasu, S. (2015) Review on Natural Dye Sensitized Solar Cells: Operation, materials and Methods. *Renewable and Sustainable Energy Reviews*, **51**, 1306-1325.

[15] Bai, Y., Mora-Seró, I., De Angelis, F., Bisquert, J. and Wang, P. (2014) Titanium Dioxide Nanomaterials for Photovoltaic Applications. *Chemical Reviews*, **114**, 10095-10130. https://doi.org/10.1021/cr400606n

[16] Diebold, U. (2003) The Surface Science of Titanium Dioxide. *Surface Science Reports*, **48**, 53-229.

[17] Zhang, J.-Y., Boyd, I.W., O'Sullivan, B.J., Hurley, P.K., Kelly, P.V. and Sénateur, J.P. (2002) Nanocrystalline TiO_2 Films Studied by Optical, XRD and FTIR Spectroscopy. *Journal of Non-Crystalline Solids*, **303**, 134-138.

[18] Turner, G., Beard, M.C. and Schmuttenmaer, C.A. (2002) Photoconductivity of Dye-Sensitized Titanium Dioxide Films Measured by Time-Resolved THz Spectroscopy. *The* 13*th International Conference on Ultrafast Phenomena*, Vancouver, 12 May 2002, ME37.

[19] Altobello, S., Bignozzi, C., Caramori, S., Larramona, G., Quici, S., Marzanni, G. and Lakhmiri, R. (2004) Sensitization of TiO_2 with Ruthenium Complexes Containing Boronic Acid Functions. *Journal of Photochemistry and Photobiology A*: *Chemistry*, **166**, 91-98.

[20] Brown, D.G., Schauer, P.A., Borau-Garcia, J., Fancy, B.R. and Berlinguette, C.P. (2013) Stabilization of Ruthenium Sensitizers to TiO_2 Surfaces through Cooperative Anchoring Groups. *Journal of the American Chemical Society*, **135**, 1692-1695. https://doi.org/10.1021/ja310965h

[21] Li, G., Yella, A., Brown, D.G., Gorelsky, S.I., Nazeeruddin, M.K., Grätzel, M., Berlinguette, C.P. and Shatruk, M. (2014) Near-IR Photoresponse of Ruthenium Dipyrrinate Terpyridine Sensitizers in the Dye-Sensitized Solar Cells. *Inorganic Chemistry*, **53**, 5417-5419. https://doi.org/10.1021/ic5006538

[22] Klein, C., Nazeeruddin, M.K., Censo, D.D., Liska, P. and Grätzel, M. (2004) Amphiphilic Ruthenium Sensitizers and Their Applications in Dye-Sensitized Solar Cells. *Inorganic Chemistry*, **43**, 4216-4226. https://doi.org/10.1021/ic049906m

[23] Hao, S., Wu, J., Huang, Y. and Lin, J. (2006) Natural Dyes as Photosensitizers for Dye-Sensitized Solar Cell. *Solar Energy*, **80**, 209-214.

[24] Narayan, M.R. (2012) Review: Dye Sensitized Solar Cells Based on Natural Photosensitizers. *Renewable and Sustainable Energy Reviews*, **16**, 208-215.

[25] Hosseinnezhad, M., Moradian, S. and Gharanjig, K. (2015) Fruit Extract Dyes as Photosensitizers in Solar Cells. *Current Science*, **109**, 953-956. https://doi.org/10.18520/cs/v109/i5/953-956

[26] Ghann, W., Chavez-Gil, T., Goede, C., Kang, H., Khan, S., Sobhi, H., Nesbitt, F. and Uddin, J. (2017) Photophysical, Electrochemical and Photovoltaic Properties of Porphyrin-Based Dye Sensitized Solar Cell. *Advances in Materials Physics and Chemistry*, **7**, 148-172.

[27] Daphnomili, D., Sharma, G.D., Biswas, S., Justin Thomas, K.R. and Coutsolelos, A.G. (2013) A New Porphyrin Bearing a Pyridinylethynyl Group as Sensitizer for Dye Sensitized Solar Cells. *Journal of Photochemistry and Photobiology A*: *Chemistry*, **253**, 88.

[28] Higashino, T. and Imahori, H. (2015) Porphyrins as Excellent Dyes for Dye-Sensitized Solar Cells: Recent Developments and Insights. *Dalton Transactions*, **44**, 448-463. https://doi.org/10.1039/C4DT02756F

[29] Hart, A.S., Chandra, B.K.C., Gobeze, H.B., Sequeira, L.R. and D'Souza, F. (2013) Porphyrin-Sensitized Solar Cells: Effect of Carboxyl Anchor Group Orientation on the Cell Performance. *ACS Applied Materials & Interfaces*, **5**, 5314-5323. https://doi.org/10.1021/am401201q

[30] Gou, F., Jiang, X., Li, B., Jing, H. and Zhu, Z. (2013) Salicylic Acid as a Tridentate Anchoring Group for Azo-Bridged Zinc Porphyrin in Dye-Sensitized Solar Cells. *ACS Applied Materials & Interfaces*, **5**, 12631-12637. https://doi.org/10.1021/am403987b

[31] Rihter, B., SriHari, S., Hunter, S. and Masnovi, J. (1993) Reactions of Alkynes and Carbene Equivalents with Oxo(Salen)Chromium(V) Complexes. *Journal of the American Chemical Society*, **115**, 3918-3924. https://doi.org/10.1021/ja00063a010

[32] Zhang, W., Loebach, J.L., Wilson, S.R. and Jacobsen, E.N. (1990) Enantioselective Epoxidation of Unfunctionalized Olefins Catalyzed by Salen Manganese Complexes. *Journal of the American Chemical Society*, **112**, 2801-2803. https://doi.org/10.1021/ja00163a052

[33] Fry, A.J. and Fry, P.F. (1993) Nickel(I) Salen-Electrocatalyzed Reduction of Benzal Chloride. *The Journal of Organic Chemistry*, **58**, 3496-3501. https://doi.org/10.1021/jo00065a008

[34] Engelmann, F.M., Losco, P., Winnischofer, H., Araki, K. and Toma, H.E. (2002) Synthesis, Electrochemistry, Spectroscopy and Photophysical Properties of a Series of Meso-Phenylpyridylporphyrins with One to Four Pyridyl Rings Coordinated to $[Ru(bipy)_2Cl]^+$ Groups. *Journal of Porphyrins and Phthalocyanines*, **6**, 33-42. https://doi.org/10.1142/S1088424602000063

[35] Amadi, L., Jenny, S.S., Ahmed, A., Brown, N., Yadav, S., Brown, D., Ghann, W., Gayrama, A., Jiru, M. and Uddin, J. (2015) Creation of Natural Dye Sensitized Solar Cell by Using Nanostructured Titanium Oxide. *Nanoscience and Nanoengineering*, **3**, 25-35. https://doi.org/10.13189/nn.2015.030301

[36] Ghann, W., Rahman, A., Rahman, A. and Uddin, J. (2016) Interaction of Sensitizing Dyes with Nanostructured TiO_2 Film in Dye-Sensitized Solar Cells Using Terahertz Spectroscopy. *Scientific Reports*, **6**, Article No. 30140. https://doi.org/10.1038/srep30140

[37] Ghann, W., Kang, H., Sheikh, T., Yadav, S., Chavez-Gil, T., Nesbitt, F. and Uddin, J. (2017) Fabrication, Optimization and Characterization of Natural Dye Sensitized Solar Cell. *Scientific Reports*, **7**, Article No. 41470. https://doi.org/10.1038/srep41470

[38] Karki, I.B., Nakarmi, J.J., Mandal, P.K. and Chatterjee, S. (2012) Absorption Spectra of Natural Dyes and Their Effect on Efficiency of ZnO Based Dye-Sensitized Solar Cells. *Nepal Journal of Science and Technology*, **13**, 179-185.

[39] Han, L., Islam, A., Chen, H., Malapaka, C., Chiranjeevi, B., Zhang, S., Yang, X. and Yanagida, M. (2012) High-Efficiency Dye-Sensitized Solar Cell with a Novel Co-Adsorbent. *Energy & Environmental Science*, **5**, 6057-6060. https://doi.org/10.1039/c2ee03418b

[40] Kurosaki, H., Matsuda, K., Yamakawa, N., Yamaguchi, Y. and Chavez-Gil, T. (2008) Crystal Structure of Chlorobis(R-1-Pyridine-2-Ylethylamine)Copper(II)Chloride. *Journal of Analytical Sciences: X-Ray Structure Analysis Online*, **24**, x305-x307.

[41] Chavez-Gil, T., Cedeño, D.L., Hamaker, C.G., Vega, M. and Rodríguez, J. (2008) Synthesis, Characterization, and Crystal Structure of [Cu{(3,5-Ph2Pz)2BH2}2]0: Evidence of a B-H-Cu Agostic Interaction. *Journal of Molecular Structure*, **888**, 168-172.

[42] Franco, E., López-Torres, E., Mendiola, M. and Sevilla, M. (2000) Synthesis, Spec-

troscopic and Cyclic Voltammetry Studies of Copper(II) Complexes with Open Chain, Cyclic and a New Macrocyclic Thiosemicarbazones. *Polyhedron*, **19**, 441-451.

[43] Benmekhbi, L., Bencharif, M., Bencharif, L. and Mosbah, S. (2011) Electrocyclization of Semicarbazone: A Novel Route of Green Synthesis of 2,5-Disubstituted-1,3,4-Oxadiazoles. *International Journal of Electrochemical Science*, **6**, 1991-2000.